Nonlinear Dyn (2018) 91:957–974
https://doi.org/10.1007/s11071-017-3921-3

ORIGINAL PAPER

A chaotic memcapacitor oscillator with two unstable equilibriums and its fractional form with engineering applications

Karthikeyan Rajagopal · Akif Akgul · Sajad Jafari · Burak Aricioglu

Received: 30 May 2017 / Accepted: 1 November 2017 / Published online: 14 November 2017

Abstract A novel charge-controlled memcapacitor 3D chaotic oscillator with two unstable equilibriums is proposed. Various dynamic properties of the proposed system are derived and investigated to show the existence of chaotic oscillations. Fractional-order analysis of the chaotic oscillator shows that the maximum value for the largest positive Lyapunov exponent is exhibited in fractional order. Adomian decomposition method is used to discretize the fractional-order system. Field-programmable gate arrays are used to realize the proposed oscillator. In addition, random number generator is designed by employing this novel chaotic system in its fractional-order form.

Keywords Memcapacitor · Bifurcation · Bicoherence · Fractional order · Circuit implementation · FPGA · RNG design

K. Rajagopal
Department of Electrical and Communication Engineering, The PNG University of Technology, Lae, Papua New Guinea
e-mail: rkarthiekeyan@gmail.com

A. Akgul · B. Aricioglu
Department of Electrical and Electronics Engineering, Faculty of Technology, Sakarya University, Sakarya, Turkey
e-mail: aakgul@sakarya.edu.tr

B. Aricioglu
e-mail: baricioglu@sakarya.edu.tr

S. Jafari
Biomedical Engineering Department, Amirkabir University of Technology, Tehran, Iran
e-mail: sajadjafari83@gmail.com

1 Introduction

Designing new chaotic systems with interesting features has attracted lots of interest recently. Some of these chaotic systems can be categorized according to their equilibria: chaotic systems with no equilibrium points [1,2], with only stable equilibria [3,4], with curves of equilibria [5], with surfaces of equilibria [6,7] and with non-hyperbolic equilibria [8,9]. Some other examples unrelated to equilibria are chaotic systems with multiscroll attractors [10–12], with multistability [13–15], with different kinds of symmetry [16–18] and with the algebraically simplest equations [19–22].

Chua [23] introduced the fourth circuit element, popularly known as memristors, in 1971. Memristors are considered to be highly nonlinear with nonvolatile characteristics and can be implemented with nanoscale technologies [24–27]. Memristor-based chaotic oscillators have been widely investigated in the recent years. Some examples are circuits with two HP memristors in antiparallel [28], a current feedback op-amp-based memristor oscillators [29] and a practical implementation of memristor-based chaotic circuits with off-the-shelf components [30]. Also memristor-based chaotic circuit for pseudorandom number generation has been analyzed in a cryptography application study [31].

Recently many researchers have discussed about fractional-order calculus and its applications [32–34]. For example, fractional-order nonlinear systems with different control approaches have been investigated [35–37], and fractional-order memristor-based no equilibrium chaotic and hyperchaotic systems are proposed [38–41].

Implementation of chaotic and hyperchaotic system using field-programmable gate arrays (FPGAs) has been widely investigated [42–44]. Chaotic random number generators have been implemented in FPGA for applications in image cryptography [45] or FPGA-implemented Duffing oscillator-based signal detectors has been proposed [46].

In the next section, we introduce a memcapacitor-based 3D chaotic oscillator with two unstable equilibriums. In Sect. 3, we analyze it carefully through dissipativity, equilibrium points, Lyapunov exponents (LE), Kaplan–Yorke (KY) dimension, bifurcation, and bicoherence in detail. Section 4 deals with the circuit implementation of the memcapacitor chaotic system. In Sects. 5 and 6, fractional-order form of chaotic memcapacitor system and its dynamic analysis are presented. Sections 7 and 8 illustrate a FPGA-based practical application and random number generator design with the fractional-order chaotic system. Finally, conclusions are given in Sect. 9.

2 Problem formulation

Many memcapacitor models with piecewise linear, quadric and cubic functions have been discussed in the literature [47–50]. Some interesting properties such as hidden attractors [51–54], coexistence attractors [55–57] and extreme multistability [58–61] were found in the memcapacitor-based chaotic oscillators.

In this study, a novel memcapacitor chaotic oscillator (NMCO) with charge-controlled memcapacitor, discussed in [62], as shown in Fig. 1 is investigated.

In Fig. 1 R, L, G and C represent resistance, inductances, conductance and capacitance, respectively. C_m is the memcapacitor as discussed in [62,63]. The current flowing through the circuit is i_G, i_R, i_{C_m}, i_L applying Kirchhoff's law to the circuit shown in Fig. 1,

$$\begin{aligned}\frac{\mathrm{d}q_{C_m}}{\mathrm{d}t} &= \frac{V_C}{R} + \left(G - \frac{1}{R}\right) V_{C_m}\\ C\frac{\mathrm{d}V_C}{\mathrm{d}t} &= \frac{(V_{C_m} - V_C)}{R} - i_L\\ L\frac{\mathrm{d}i_L}{\mathrm{d}t} &= V_C\end{aligned} \tag{1}$$

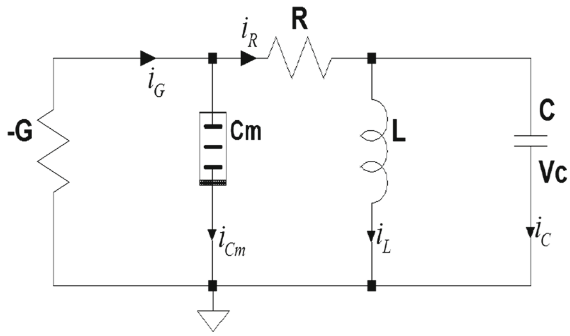

Fig. 1 Memcapacitor-based chaotic oscillator

where q_{C_m} represents the memcapacitor charge, and V_C and V_{Cm} represent voltage across capacitor and memcapacitor, respectively. Voltage of a charge-controlled memcapacitor can be written as:

$$V_{C_m} = (\alpha - \beta\sigma)q_{C_m} \tag{2}$$

where α and β are memcapacitor parameters such that $\alpha - \beta\sigma$ is the inverse of memcapacitance (C_m^{-1}) and $\sigma = \sigma_0 + \int_t^\int t_0(t)\mathrm{d}t$. If Eq. (2) is substituted into Eq. (1), it can be seen that Eq. (1) has four state variables namely: q_{C_m}, V_C, σ and i_L. If the initial value of σ is taken very small (i.e., close to zero), then $\sigma \approx \int_{t_0}^t q_{cm}(t)\mathrm{d}t$. By taking time integral of Eq. (1), the number of state variable can be reduced to three. The time integral of Eq. (1) is

$$\begin{aligned}\frac{\mathrm{d}\sigma}{\mathrm{d}t} &= \frac{\varphi_C}{R} + \left(G - \frac{1}{R}\right)\varphi_{C_m}\\ C\frac{\mathrm{d}\varphi_C}{\mathrm{d}t} &= \frac{(\varphi_{C_m} - \varphi_C)}{R} - q_L\\ L\frac{\mathrm{d}q_L}{\mathrm{d}t} &= \varphi_C\end{aligned} \tag{3}$$

where $\sigma \approx \int_{t_0}^t q_{cm}(t)\mathrm{d}t$, $\varphi_c = \int v_c(t)\mathrm{d}t$, $\varphi c_m = \int v_m(t)\mathrm{d}t$ and $q_L = \int \imath_L(t)\mathrm{d}t$.

The time integral of memcapacitor voltage can be written as:

$$\varphi c_m = \int v c_m(t)\mathrm{d}t = \alpha\sigma - \frac{1}{2}\beta\sigma^2 \tag{4}$$

By substituting time integral of memcapacitor voltage given in Eq. (4) into Eq. (3), the following equation system is obtained

$$\begin{aligned}\frac{\mathrm{d}\sigma}{\mathrm{d}t} &= \frac{\varphi_C}{R} + \left(G - \frac{1}{R}\right)\left(\alpha\sigma - \frac{1}{2}\beta\sigma^2\right)\\ C\frac{\mathrm{d}\varphi_C}{\mathrm{d}t} &= \frac{\left(\alpha\sigma - \frac{1}{2}\beta\sigma^2 - \varphi_C\right)}{R} - q_L\\ L\frac{\mathrm{d}q_L}{\mathrm{d}t} &= \varphi_C\end{aligned} \tag{5}$$

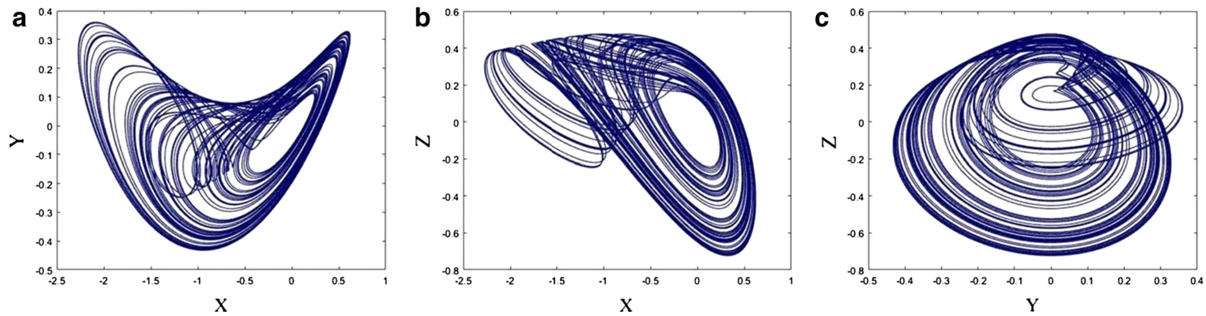

Fig. 2 **a** $x-y$ plane, **b** $x-z$ plane and **c** $y-z$ plane phase portraits of system (3) when $a_1 = 1.638$, $a_2 = -0.963$, $a_3 = 4.5$, $a_4 = 0.7$, $a_5 = -0.4$ and $a_6 = -1.75$

The state variables of Eq. (5) are σ, φ_C and q_L. Let us define new state variables as $x = \sigma$, $y = \varphi_c$ and $z = -Rq_L$ and let us define $\tau = \frac{t}{RC}$.

$$\frac{dx}{d\tau} = a_1x + a_2x^2 + a_3y$$
$$\frac{dy}{d\tau} = a_4x + a_5x^2 - y + z$$
$$\frac{dz}{d\tau} = a_6y \tag{6}$$

where the parameters are defined as $a_1 = C\alpha(RG-1)$, $a_2 = -\frac{C\beta}{2}(RG-1)$, $a_3 = C$, $a_4 = \alpha$, $a_5 = -\frac{\beta}{2}$, $a_6 = -\frac{R^2C}{L}$ and for the values of $L = 0.13H$, $C = 3.57F$, $G = 2.1$, $?R = 211\Omega$, $\alpha = 0.7F^{-1}$ and $\beta = 0.8F^{-1}c^{-1}s^{-1}$, and the NMCO system shows chaotic oscillations and the corresponding parameter values are derived as, $a_1 = 1.638$, $a_2 = -0.936$, $a_3 = 4.5$, $a_4 = 0.7$, $a_5 = -0.4$ and $a_6 = -1.75$. The initial conditions are chosen as [0.001, 0.001, 0.001]. Figure 2 shows the 2D phase portraits of system (6).

3 Dynamic analysis of hyperchaotic memcapacitor oscillator (NMCO)

The dynamic properties of the NMCO system namely dissipativity, equilibrium points, eigenvalues, Lyapunov exponents (LE) and Kaplan–Yorke (KY) dimension are derived and discussed in this section.

3.1 Dissipativity, equilibrium points, Lyapunov exponents and Kaplan–Yorke dimension

The divergence of Eq. (3) is

$$\frac{\partial x}{\partial x} + \frac{\partial y}{\partial y} + \frac{\partial z}{\partial z} = a_1 + 2a_2x - 1 \tag{7}$$

This shows that it is dissipative if $<x>$ be smaller than $\frac{1-a_1}{2a_2}$, where $<x>$ represents the arithmetic average of x. Hence, the system volume is going to be reduced to zero, and the NMCO system (3) converges to a strange attractor of the system asymptotically. By equating $X = 0$, the NMCO system (3) shows two equilibrium points $E_1 = [0, 0, 0]$ and $E_2 = [-a_1/a_2, 0, 0]$. By calculating the characteristic equation of the system, it can be seen that both equilibria are unstable. The Jacobian method is employed in calculation of the LEs of the NMCO system. The numerical value of LEs of the NMCO system are

$$L_1 = 0.105, L_2 = 0, L_3 = -2.1734 \tag{8}$$

Since there is a positive LE in (5), the NMCO system (3) has chaotic solutions. The sum of LEs of the NMCO system (3) is given below which is negative.

$$L_1 + L_2 + L_3 = -2.065 < 0 \tag{9}$$

The dissipativity of the NMCO system (3) can be shown with Eq. (6). The KY dimension of the NMCO system (3) is

$$D_{KY} = 2 + \frac{L_1 + L_2}{|L_3|} = 2.048, \tag{10}$$

which is fractional.

3.2 Bifurcation

To understand the parameter dependence of the NMCO system, we derive and investigate the bifurcation plots. By changing all of its six parameters, this NMCO system exhibits a familiar period doubling to enter chaos. However, for simplicity, only bifurcation diagram and Lyapunov exponents diagram with changing parameter a_1 are shown in Fig. 3.

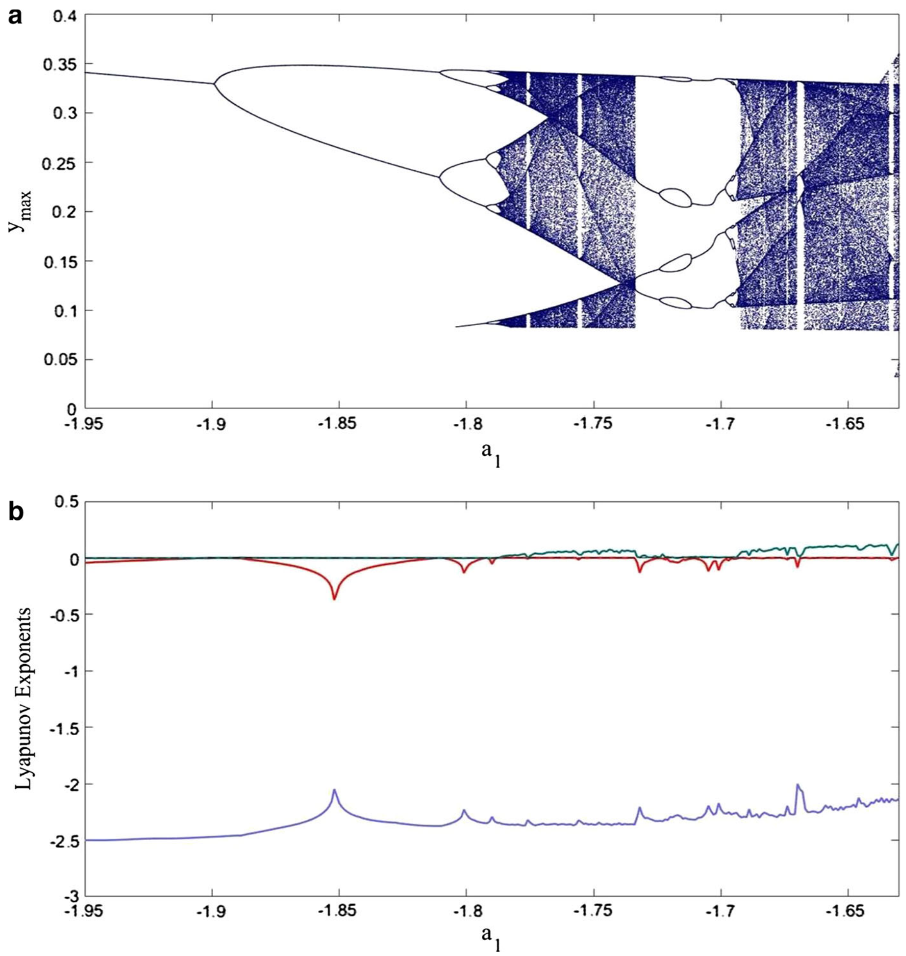

Fig. 3 **a** Bifurcation diagram of system (3) with respect to parameter a_1 (y_{max} are the local maxima of y signal and the initial values are (0.1, 0.1, 0.1)) and **b** Lyapunov exponents of system (3) with respect to parameter a_1. The rest of the parameters are $a_2 = -0.963$, $a_3 = 4.5$, $a_4 = 0.7$, $a_5 = -0.4$ and $a_6 = -1.75$

3.3 Bicoherence

Higher-order spectra have been used to study the non-linear interactions between frequency modes [64,65]. Let $x(t)$ be a stationary random process defined as,

$$x(t) = \sum_{n=1}^{N} A_n e^{j\omega_n t} + A_n^* e^{-j\omega_n t} \tag{11}$$

where w is the angular frequency, n is the frequency modal index and A_n are the complex Fourier coefficients. The power spectrum can be defined as,

$$P(\omega_k) = E[A_{\omega_k} A_{\omega_k}^*] \tag{12}$$

and discrete bispectrum can be defined as,

$$B(\omega_k, \omega_j) = E[A_{\omega_k} A_{\omega_j} A_{\omega_k+\omega_j}^*] \tag{13}$$

If the modes are independent, then the average triple products of Fourier components is zero resulting in a zero bispectrum [64]. The study of bicoherence is to give an indication of the relative degree of phase coupling between triads of frequency components. There are two main reasons to employ bicoherence analysis. The first one is obtaining information about deviations due to Gaussianity and suppressing colored Gaussian noise. The second one is that signals with asymmetric nonlinearities can be detected and identified with bicoherence analysis. It is a third-order spectrum as it can be seen in Eq. (10), while as it can be seen in Eq. (9) power spectrum is a second order. Power spectrum and bispectrum can be defined as $X'(f) * X(f)$ and $X(f_j) * X(f_k) * X'(f_j + f_k)$, respectively, where $X(f)$ represents Fourier transform of $x(t)$ and $X'(f)$ represents Fourier transform of conjugate of $x(t)$. It can be understood that the bispectrum is a complex function of two frequencies (f_j, f_k). Bicoherence is square of amplitude. To calculate the bispectrum, the time series are divided into M parts and each part has length of N.

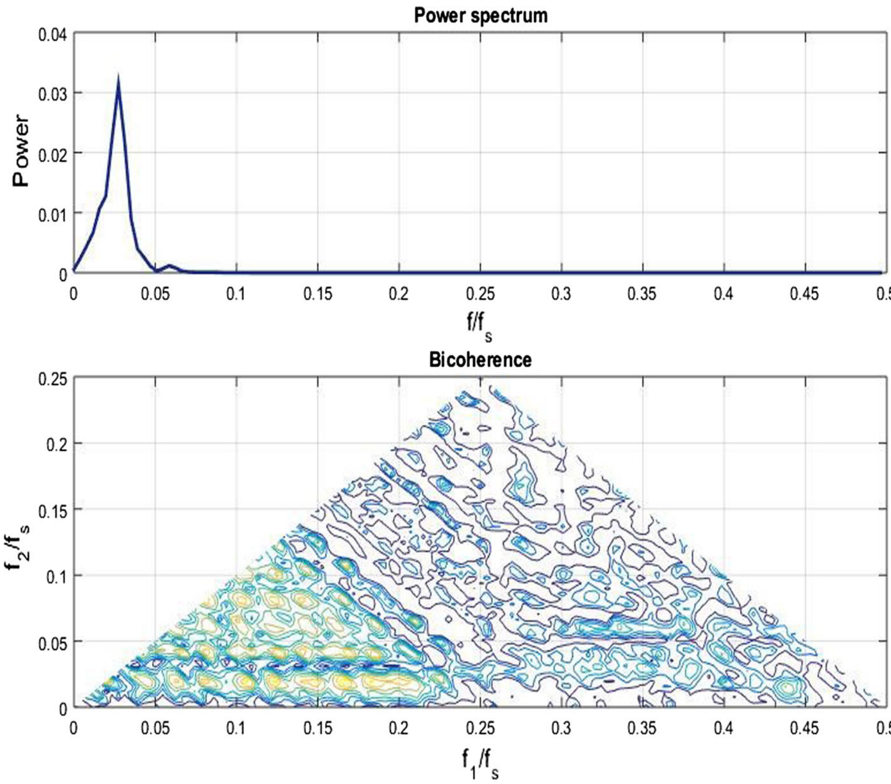

Fig. 4 Bicoherence plot of NMCO system for state x with sampling frequency of 1.5 KHz

Then, their Fourier transforms and biperiodogram are calculated. Finally, they are averaged over all segments. Although the inputs of bicoherence functions are two different frequencies and their summation, the output of the function is one-dimensional. Hence, bicoherence can be considered as a function of sum of two frequencies. Pezeshki [66] gives autobispectrum of a chaotic system. Autobispectrum is calculated from the Fourier coefficients.

$$B(\omega_1, \omega_2) = E[A(\omega_1)A(\omega_2)A^*(\omega_1 + \omega_2)] \tag{14}$$

where w_n is the radian frequency and A is the Fourier coefficients. The square of bicoherence can be written as

$$b(\omega_1, \omega_2) = |B(\omega_1, \omega_2)|^2 / P(\omega_1)P(\omega_2)P(\omega_1 + \omega_2) \tag{15}$$

where $P(\omega_1)$ and $P(\omega_2)$ are the power spectrums at f_1 and f_2.

Figures 4 and 5 show the bicoherence contours of the FONMCO system for state x and all states together, respectively. Yellow-colored parts show the multifrequency components contributing to the power spectrum. As it is shown in Figs. 4 and 5, the cross-bicoherence is nonzero and non-constant; hence, the state relationship is nonlinear. As shown in Fig. 4, the spectral power is very low as compared to the spectral power of all states together (Fig. 5) indicating the existence of multifrequency nodes. Also Fig. 5 shows the nonlinear coupling (straight lines connecting multiple frequency terms) between the states. The yellow shades/lines and non-sharpness of the peaks and the structure around the origin in figures indicate that the nonlinear relation of the states x, y, z is not of the quadratic nonlinearity. The most two dominant frequencies (f_1, f_2) are selected to obtain bicoherence contour. As a reference frequency, the sampling frequency (f_s) is selected. To derive the power spectrum for individual frequencies, direct FFT is used and Hankel operator is used as the frequency mask. Hanning window is used as the FIR filter to separate the frequencies [40].

4 Circuit implementation of the memcapacitor chaotic system

There are many works in the literature related to electronic circuit designs [67–77]. In this section, the cir-

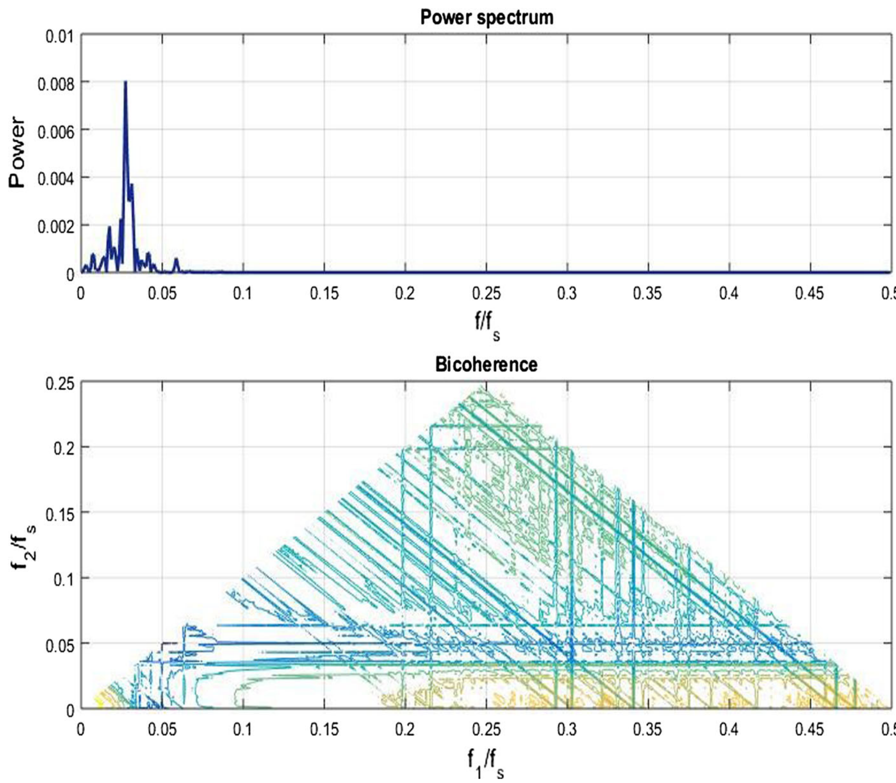

Fig. 5 Bicoherence plot of NMCO system for all states with sampling frequency of 1.5 KHz

cuit design of memcapacitor chaotic system (3) is differently implemented in the oscilloscope as real-time engineering application. The chaotic memcapacitor in this work has been exhibited noise-like behaviors because its signal values are very low as shown in Fig. 2. So, chaotic system are firstly scaled to increase the signal values for electronic circuit application.

For scaling process, let $X = 5x$, $Y = 5y$, $Z = 5z$, and then, setting the original state variables x, y, z as X, Y, Z the scaled chaotic memcapacitor system becomes as follows.

$$\left\{\begin{array}{ll} \dot{x} = a_1x + a_2x^2 + a_3y & X = 5x \\ \dot{y} = a_4x + a_5x^2 - y + z \Rightarrow & Y = 5y \\ \dot{z} = a_6y & Z = 5z \end{array}\right\} \Rightarrow \begin{array}{l} x = X/5 \\ y = Y/5 \\ z = Z/5 \end{array} \tag{16}$$

$$X = 5x, \quad Y = 5y, \quad Z = 5z \tag{17}$$

Finally, scaled chaotic memcapacitor system are given by

$$\begin{aligned} \dot{X} &= a_1X + \frac{a_2X^2}{5} + a_3Y \\ \dot{Y} &= a_4X + \frac{a_5X^2}{5} - Y + Z \\ \dot{Z} &= a_6Y \end{aligned} \tag{18}$$

In Fig. 6 are shown the new phase portraits of scaled memcapacitor oscillator with increased amplitude values. After these processes, we can do electronic circuit design as real-time application.

The designed electronic circuit of the scaled memcapacitor chaotic system is given in Fig. 7. The circuit consists of basic electronic components such as resistors, capacitor, op-amps and multipliers.

R1 = 244 kΩ, R2 = 213 kΩ, R3 = 89 kΩ, R4 = R5 = 100 kΩ, R6 = 570 kΩ, R7 = 500 *k*Ω, R8 = R9 = 400 kΩ, R10 = R11 = 100 kΩ, R13 = 228 kΩ, R14 = R15 = 100 kΩ, C1 = C2 = C3 = 1 nF, Vn = − 15 V, Vp = 15 V were chosen. The oscilloscope outputs of memcapacitor chaotic system are shown in Fig. 8 for $x - y$, $x - z$ and $y - z$ planes.

Also, the experimental circuit of the chaotic memcapacitor circuit is shown in electronic card in Fig. 9 for $x - z$ plane.

5 Fractional-order NMCO system (FONMCO)

In this section, modeling of the fractional-order form of the hyperchaotic memcapacitor oscillator (FON-

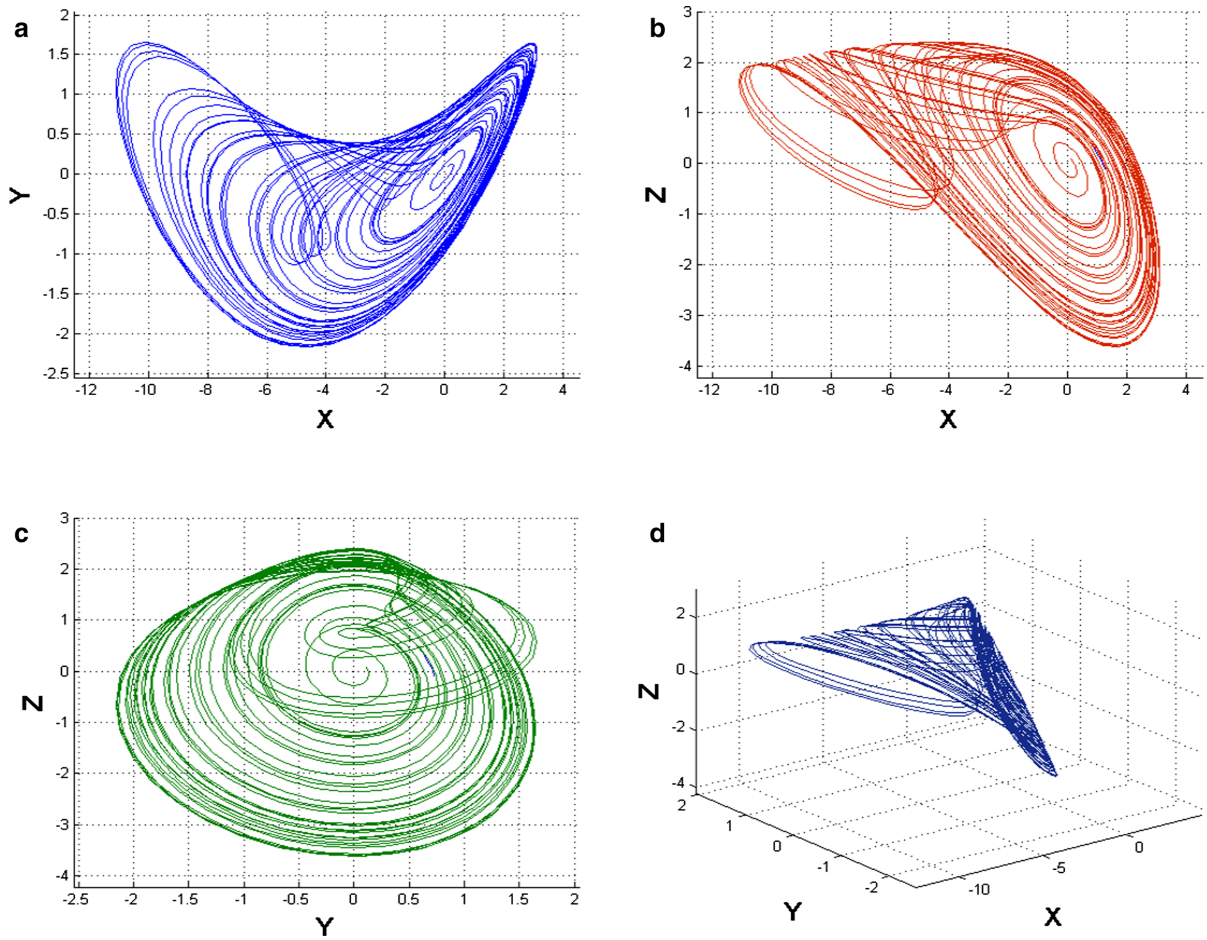

Fig. 6 2D and 3D phase portraits of the scaled memcapacitor oscillator (3): **a** $x - y$, **b** $x - z$, **c** $y - z$, **d** $x - y - z$

MCO) is introduced. Grunwald–Letnikov, Riemann–Liouville and Caputo [32–34] are the usually employed methods for the fractional-order differential operator. In the study, Grunwald–Letnikov (GL) method is employed and given as

$$ {}_aD_t^q f(t) = \lim_{h\to 0}\left\{\frac{1}{h^q}\sum_{j=0}^{\left[\frac{t-q}{h}\right]}(-1)^j\binom{q}{j} f(t-jh)\right\} = \lim_{h\to 0}\left\{\frac{1}{h^q}\Delta_h^q f(t)\right\} \quad (19)$$

where D refers to the fractional-order generalization, $\Delta_h^q f(t)$ is generalized difference, h is the step size, a and t are limits, and q is the fractional order of the differential equation.

Equation (16) can be written as

$$ {}_{(t-L)}D_t^q f(t) = \lim_{h\to 0}\left\{h^{-q}\sum_{j=0}^{N(t)} b_j\,(f(t-jh)\right\} \quad (20)$$

where b_j is binomial and given as

$$ b_j = \left(1 - \frac{a+q}{j}\right) b_{j-1} \quad (21)$$

In theory, calculation of fractional-order differential equation requires use of infinite memory, but in practice, the equation given below is used for the calculation.

$$ N(t) = \min\left\{\left[\frac{t}{h}\right], \left[\frac{L}{h}\right]\right\} \quad (22)$$

where L and h represents the memory length sampling time, respectively.

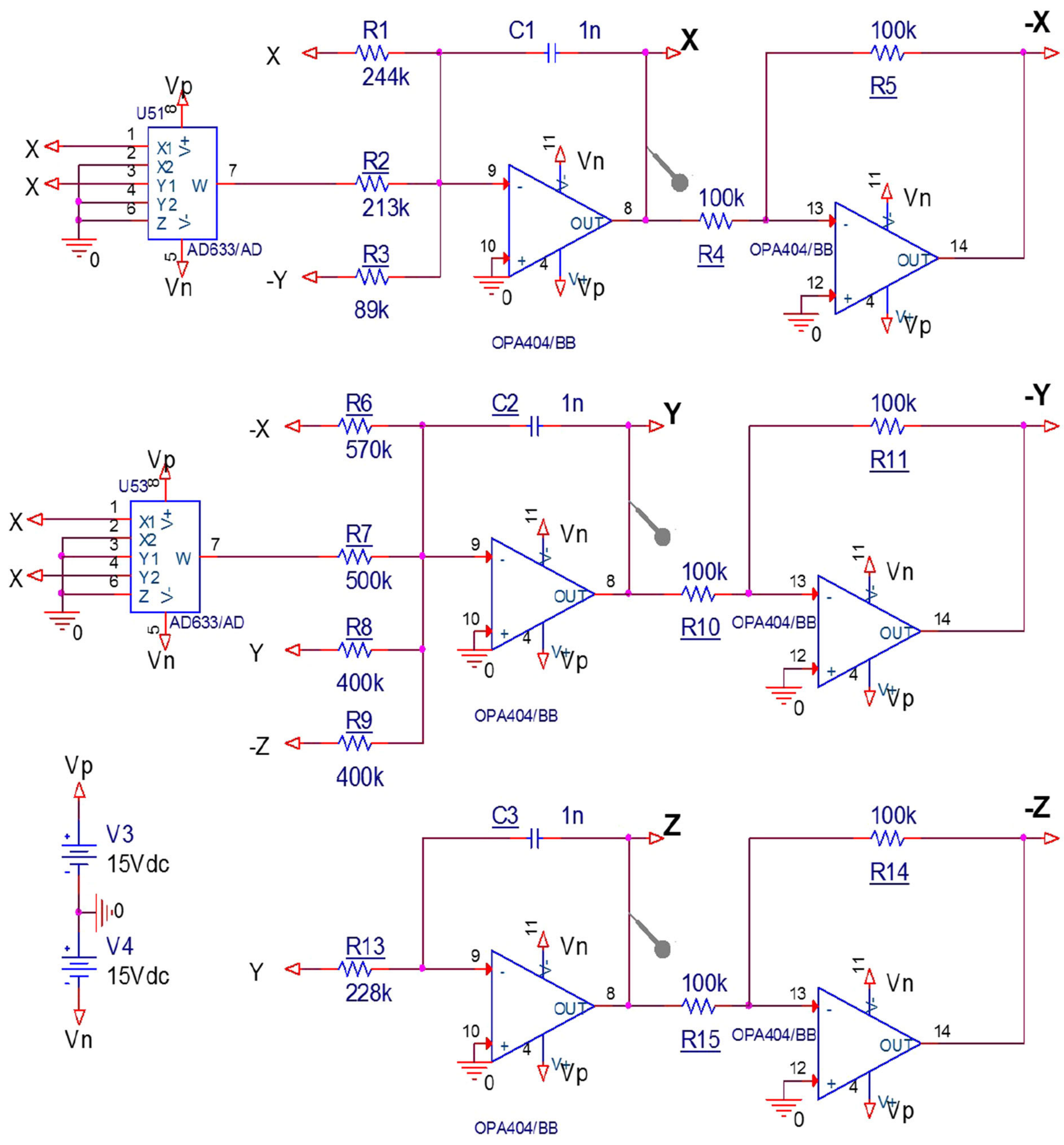

Fig. 7 Electronic circuit of the scaled chaotic memcapacitor system

Using (16)–(19), the FONMCO system is derived as,

$$\frac{\mathrm{d}^{q_x} x}{\mathrm{d}t^{q_x}} = a_1 x + a_2 x^2 + a_3 y$$

$$\frac{\mathrm{d}^{q_y} y}{\mathrm{d}t^{q_y}} = a_4 x + a_5 x^2 - y + z$$

$$\frac{\mathrm{d}^{q_z} z}{\mathrm{d}t^{q_z}} = a_6 y \tag{23}$$

where q_x, q_y, q_z are the fractional orders of the FONMCO system. The 2D phase portraits of the FONMCO system is given Fig. 10. The system parameters and the initial values are as same as in the system discussed in Sect. 2.

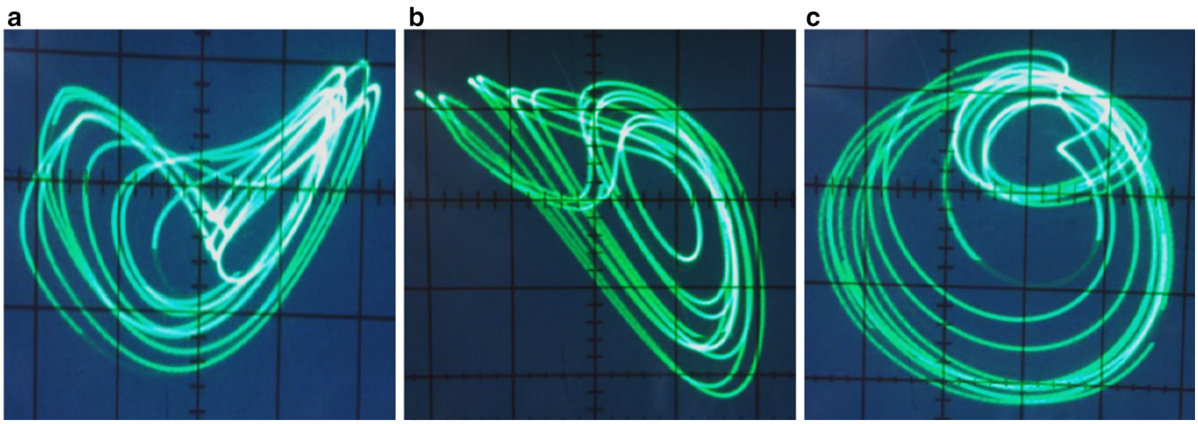

Fig. 8 2D phase portraits of the chaotic memcapacitor on the oscilloscope. The initial conditions and parameter values are taken as in Sect. 2: **a** $x - y$, **b** $x - z$, **c** $y - z$

Fig. 9 Experimental circuit of the chaotic memcapacitor circuit

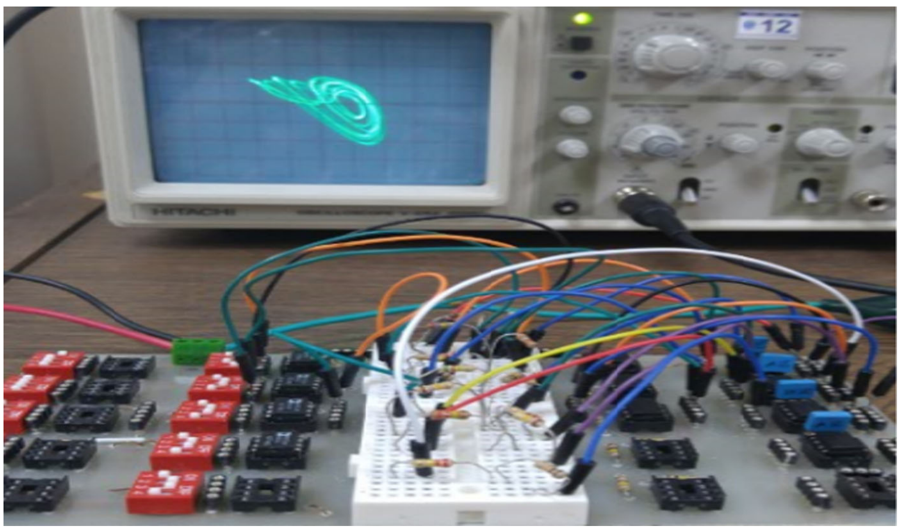

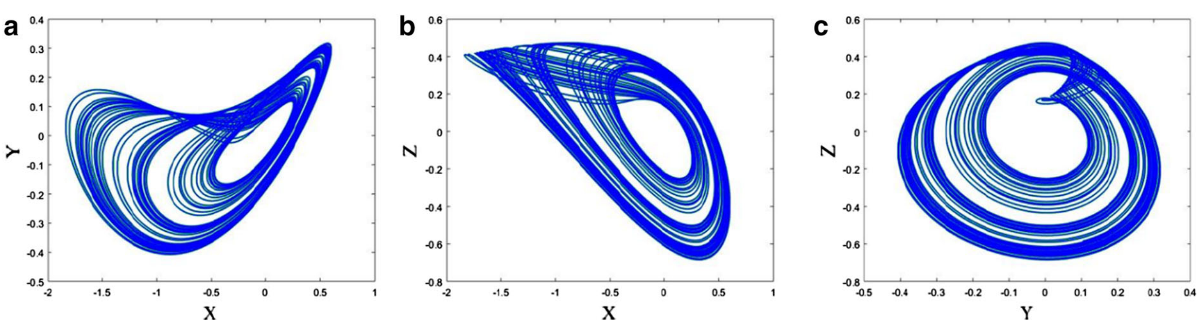

Fig. 10 2D phase portraits of the FONMCO system, $q = 0.992$

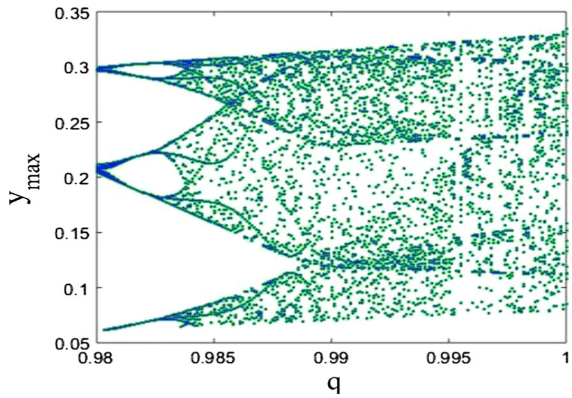

Fig. 11 Fractional-order bifurcation plot

6 Dynamic analysis of the FONMCO chaotic systems

6.1 Bifurcation with fractional order

Some of the FONMCO system dynamic properties such as LEs and bifurcation remain similar to the that of the NMCO chaotic systems [38,39] if $q_x, q_y, q_z > 0.983$. For a fractional-order system, investigation of bifurcation with fractional order is very important. As shown in Fig. 11, bifurcation of the FONMCO system for change in fractional order shows that the systems' chaotic oscillations remain if $q_i > 0.983$ and when $q = 0.992$ the largest positive Lyapunov exponent is $L_1 = 0.118$, while for the integer-order case the largest Lyapunov exponent is $L_1 = 0.105$. Figure 12a–f shows the 2D phase portraits in $X - Y$ plane for different fractional orders.

6.2 Stability analysis

6.2.1 Commensurate order

For a q-order commensurate FONMCO system, the system shows chaotic oscillations if

$$|\arg(\text{eig}(J_E))| = |\arg(\lambda_i)| > \frac{q\pi}{2}$$

where J_E is the Jacobian matrix at the equilibrium E and λ_i are the eigenvalues of the FONMCO system for $i = 1, 2, 3$. The eigenvalues must be in the unstable region and stability condition for the FONMCO system is $q > \frac{2}{\pi}\tan^{-1}\left(\frac{|\text{Im}\lambda|}{\text{Re}\lambda}\right)$. The NMCO system shows two equilibrium at $E_1 = [0, 0, 0]$ and $E_2 = [-1.75, 0, 0]$, and the characteristic equation for the commensurate orders $q = 0.99$ for the equilibrium point E_1 is given by $\lambda^{297} + 3\lambda^{199} + 2.638\lambda^{198} + 3\lambda^{101} + 5.276\lambda^{100} + 0.238\lambda^{99} + \lambda^3 + 2.638\lambda^2 + 0.238\lambda + 2.8665$ and at E_2 is $\lambda^{297} + 3\lambda^{199} - 0.638\lambda^{198} + 3\lambda^{101} - 1.276\lambda^{100} + 3.262\lambda^{99} + \lambda^3 - 0.638\lambda^2 + 3.262\lambda - 2.8665$.

6.2.2 Incommensurate order

The FONMCO system shows chaotic oscillations for the given condition below.

$$\frac{\pi}{2M} - \min_i(|\arg(\lambda i)|) > 0$$

where M is the least common multiple (LCM) of the fractional orders. If $q_x = 0.99, q_y = 0.99, q_z = 0.98, q_w = 0.98$, then $M = 100$. The characteristic equation of the system at the equilibriums is $\det(\text{diag}[\lambda^{Mq_x}, \lambda^{Mq_y}, \lambda^{Mq_z}] - J_E) = 0$; then, we get $\det(\text{diag}[\lambda^{99}, \lambda^{99}, \lambda^{98}] - J_E) = 0$ and the characteristic equation at equilibrium point E_1 is $\lambda^{296} + \lambda^{199} + 3\lambda^{198} + 1.638\lambda^{197} + 2\lambda^{101} + 4.638\lambda^{100} + 1.876\lambda^{99} + \lambda^3 + 2.638\lambda^2 + 0.238\lambda + 2.8665$ and at the equilibrium point E_2 is $\lambda^{296} + \lambda^{199} + 3\lambda^{198} - 1.638\lambda^{197} + 2\lambda^{101} + 1.362\lambda^{100} + 1.624\lambda^{99} + \lambda^3 - 0.638\lambda^2 + 3.262\lambda - 2.8665$. For the values of parameters mentioned in Sect. 2, the solution of the characteristic equation is approximated to $\lambda_{296} = 1.848$ and whose argument is zero and which is the minimum argument, and hence, the stability necessary condition becomes $\frac{\pi}{200} - 0 > 0$ which solves for $0.0157 > 0$.

7 FPGA implementation of the FONMCO systems

The three main approaches to solve fractional-order chaotic systems are frequency-domain method [78], Adomian decomposition method (ADM) [79] and Adams–Bashforth–Moulton (ABM) algorithm [80]. Among these three methods, ADM is the most advantageous one for obtaining accurate results with less computational power [81,82]. Hence, the proposed FONMCO system is implemented in FPGA by applying ADM scheme. The most challenging issue in the FPGA realization of the FONMCO system is that there is no available block for the fractional-order integrator in the system generator [39–41]. Because the ADM algorithm converges fast [82,83], for obtaining FONMCO system solution the first 6 terms are taken. For real cases, it is impossible to find the accurate value of x when t takes

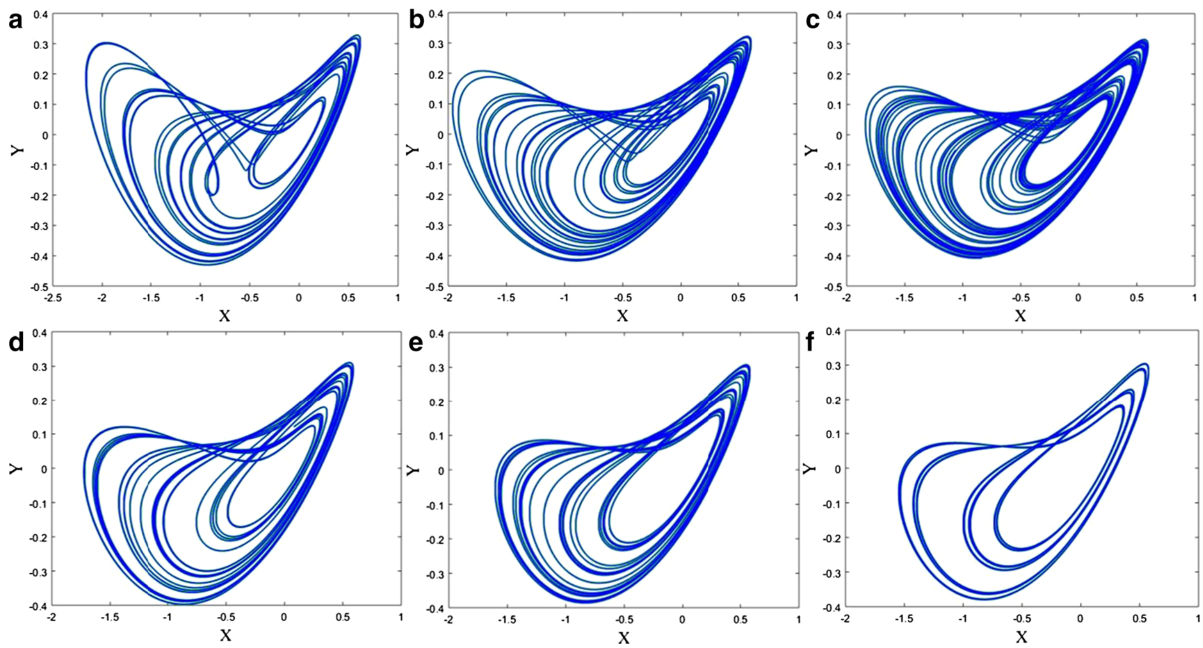

Fig. 12 2D phase portrait ($X-Y$ plane) of FONMCO system for different fractional orders **a** $q=0.999$, **b** $q=0.995$, **c** $q=0.992$, **d** $q=0.990$, **e** $q=0.985$, **f** $q=0.983$

larger values [84]. Hence, a discretization method in time is designed. That is to say, for a time interval of ti (initial time) to tf (final time), we divide the interval into (tn, tn+1) and we get the value of $x(n+1)$ at time tn $+$ 1 by applying $x(n)$ at time $t_n n$ using the relation $x(n+1)=F(x(n))$ [84]. We use the ADM method [79,84] to discretize the fractional-order CA system for implementing in FPGA. The fractional-order discrete form of the dimensionless state equations for the FONMCO system can be given as,

$$x_{n+1}=\sum_{j=0}^{6} p_1^j \frac{h^{jq}}{\Gamma(jq+1)}$$
$$y_{n+1}=\sum_{j=0}^{6} p_2^j \frac{h^{jq}}{\Gamma(jq+1)}$$
$$z_{n+1}=\sum_{j=0}^{6} p_3^j \frac{h^{jq}}{\Gamma(jq+1)} \quad (24)$$

where p_i^j are the Adomian polynomials with $i=1,2,3$ and $p_1^0=x_n$, $p_2^0=y_n$, $p_3^0=z_n$. The Adomian first polynomial is derived as,

$$p_1^1=a_1 p_1^0+a_2 p_1^0 p_1^0+a_3 p_{2^0}$$
$$p_2^1=a_4 p_1^0+a_5 p_1^0 p_1^0-p_2^0+p_{3^0}$$
$$p_3^1=a_6 p_{2^0} \quad (25)$$

The Adomian second polynomial is derived as,

$$p_1^2=a_1 p_1^1+a_2\left[p_1^0 p_1^1+p_1^1 p_{1^0}\right]+a_3 p_{2^1}$$
$$p_2^2=a_4 p_1^1+a_5\left[p_1^0 p_1^1+p_1^1 p_{1^0}\right]-p_2^1+p_{3^1}$$
$$p_3^2=a_6+p_{2^1} \quad (26)$$

The Adomian third polynomial is derived as,

$$p_1^3=a_1 p_1^2+a_2\left[p_1^0 p_1^2+p_1^2 p_1^0 + \frac{\Gamma(2q+1)}{\Gamma^2(q+1)}\left[p_1^1 p_1^1+p_1^1 p_1^1\right]\right]+a_3 p_{2^2}$$
$$p_2^3=a_4 p_1^2+a_5\left[p_1^0 p_1^2+p_1^2 p_1^0 + \frac{\Gamma(2q+1)}{\Gamma^2(q+1)}\left[p_1^1 p_1^1+p_1^1 p_1^1\right]\right]-p_2^2+p_{3^2}$$
$$p_3^3=a_6 p_{2^2} \quad (27)$$

The Adomian fourth polynomial is derived as,

$$p_1^4=a_1 p_1^3+a_2\left[p_1^0 p_1^3+p_1^3 p_1^0 + \frac{\Gamma(3q+1)}{\Gamma(q+1)\Gamma(2q+1)}\left[p_1^2 p_1^1+p_1^2 p_{1^1}\right]\right]$$
$$p_2^4=a_4 p_1^3+a_5\left[p_1^0 p_1^3+p_1^3 p_1^0\right.$$

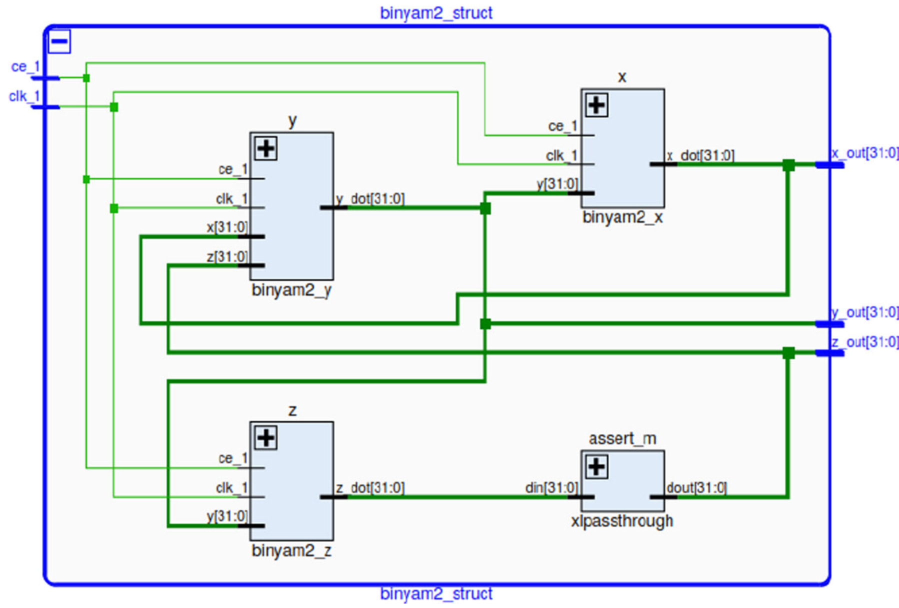

Fig. 13 RTL schematics of the FONMCO system implemented in Kintex 7 (Device = $7k160t$ Package = fbg484 S). The sampling time of the system is kept at 0.01 s to minimize the time slack errors. The entire system is configured for a 32-bit operation

$$+\frac{\Gamma(3q+1)}{\Gamma(q+1)\Gamma(2q+1)}\left[p_1^2 p_1^1 + p_1^2 p_{1^1}\right]\Big]$$
$$- p_2^3 + p_{3^3}$$
$$p_3^4 = a_6 p_{2^3} \tag{28}$$

The Adomian fifth polynomial is derived as,

$$p_1^5 = a_1 p_1^4 + a_2\Big[p_1^4 p_1^0 + p_1^0 p_1^4$$
$$+\frac{\Gamma(4q+1)}{\Gamma(q+1)\Gamma(3q+1)}\left[p_1^3 p_1^1 + p_1^1 p_{1^3}\right]\Big]$$
$$+ a_3 p_{2^4}$$
$$p_2^5 = a_4 p_1^4 + a_5\Big[p_1^4 p_1^0 + p_1^0 p_1^4$$
$$+\frac{\Gamma(4q+1)}{\Gamma(q+1)\Gamma(3q+1)}\left[p_1^3 p_1^1 + p_1^1 p_{1^3}\right]\Big]$$
$$-p_2^4 + p_3^4$$
$$p_3^5 = a_6 p_2^4 \tag{29}$$

The Adomian sixth polynomial is derived as,

$$p_1^6 = a_1 p_1^5 + a_2\Big[p_1^5 p_1^0 + p_1^0 p_1^5$$
$$+\frac{\Gamma(5q+1)}{\Gamma(q+1)\Gamma(4q+1)}\left[p_1^4 p_1^1 + p_1^1 p_1^4\right]\Big]$$
$$+ a_3 p_{2^5}$$
$$p_2^6 = a_4 p_1^5 + a_5\Big[p_1^5 p_1^0 + p_1^0 p_1^5$$
$$+\frac{\Gamma(5q+1)}{\Gamma(q+1)\Gamma(4q+1)}\left[p_1^4 p_1^1 + p_1^1 p_1^4\right]\Big]$$
$$- p_2^5 + p_{3^5}$$
$$p_3^6 = a_6 p_{2^5} \tag{30}$$

where $h = tn + 1 - tn$ and $\Gamma(\dot{})$ is the gamma function. The fractional-order discretized system (21) is then implemented in FPGA, and the necessary Adomian polynomials are calculated using (22)–(27). For implementing in FPGA, the value of h is taken as 0.001 s and the initial values are fed into the forward register with fractional order $q = 0.992$ for FONMCO system. Figure 13 shows the RTL schematics of the FONMCO system implemented in Kintex 7. Figure 14a shows the power consumed by FONMCO system for order $q = 0.992$, and Fig. 14b shows the power consumed for various fractional orders and it can be seen that maximum power is consumed when the FONMCO system exhibits the largest Lyapunov exponent. Table 1 shows the resources consumed with the consumed clock frequencies, and Fig. 15 shows the 2D phase portraits of the FPGA-implemented FONMCO system.

8 Random number generator with FONMCO system

Random numbers are used in many areas, e.g., video games, encryption, drawing of lots and weather forecast simulations [85–87]. In the literature, jitter [88], metastable [89] and chaotic systems [70,72,76,90–95] are also used as a source of entropy. In the paper, a design of random number generator (RNG) is realized

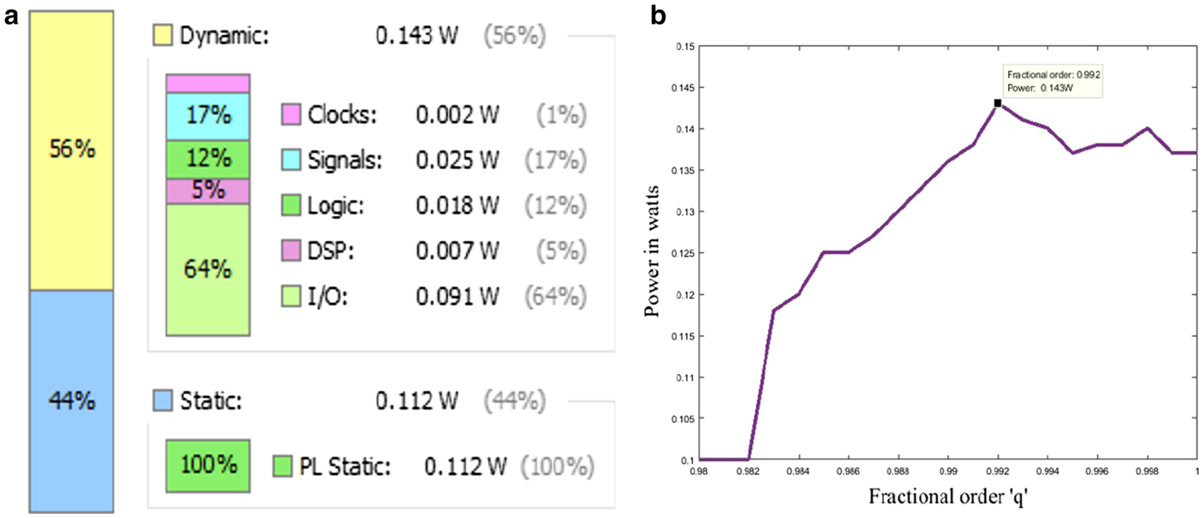

Fig. 14 **a** Power consumed by FONMCO system for $q = 0.998$, **b** power consumed by FONMCO system for various fractional orders. It can be seen that maximum power of 0.204 W is consumed for order $q = 0.998$ when the FONMCO system shows the largest Lyapunov exponents

Table 1 Resource consumption of FPGA-implemented FONMCO system

Resource	Utilization	Available	Utilization (%)	Clock frequency Available (Mhz)	Used (Mhz)
LUT	1220	101,400	1.20	500	188
FF	192	202,800	0.09	500	162
DSP	8	600	1.33	250	97
IO	97	285	34.04	300	115
BUFG	1	32	3.13	300	87

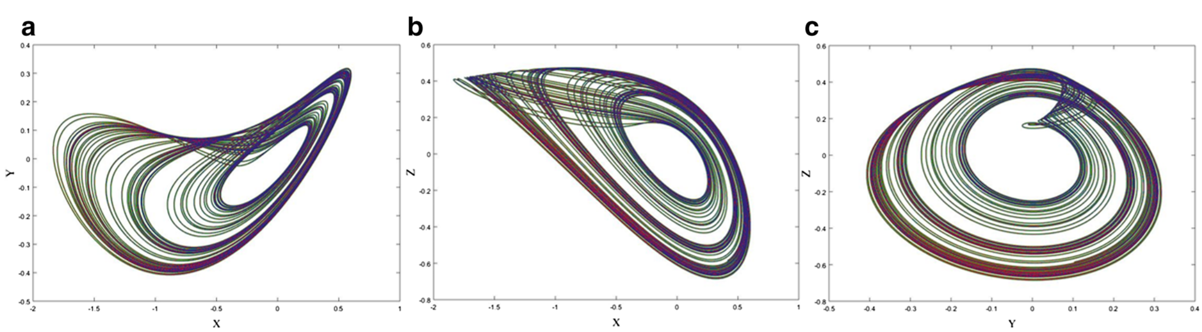

Fig. 15 2D phase portraits of the FPGA-implemented FONMCO system. The initial conditions and parameter values are taken as in Sect. 2, and the order of the system is $q = 0.992$; **a** X–Y plane, **b** X–Z plane, **c** Y–Z plane

Table 2 NIST-800-22 test results of 3D memcapacitor chaotic system-based RNG

NIST statistical tests	*P*-value (*X*)	*P*-value (*Y*)	*P*-value (*Z*)	Result
Frequency (monobit) test	0.1056	0.4839	0.4952	Passed
Block-frequency test	0.5412	0.8796	0.4001	Passed
Cumulative-sum test	0.1775	0.3271	0.6904	Passed
Runs test	0.9803	0.9732	0.7335	Passed
Longest run test	0.7585	0.8621	0.3281	Passed
Binary matrix rank test	0.4237	0.9268	0.8370	Passed
Discrete fourier transform test	0.6332	0.4741	0.5029	Passed
Non-overlapping templates test	0.0276	0.2708	0.0352	Passed
Overlapping, templates test	0.6090	0.3848	0.4222	Passed
Maurer's universal statistical test	0.3216	0.8306	0.0373	Passed
Approximate entropy test	0.6010	0.4870	0.8824	Passed
Random-excursion test	0.2640	0.7444	0.1577	Passed
Random-excursion variant test	0.7681	0.5860	0.4165	Passed
Serial test 1	0.8636	0.4839	0.2218	Passed
Serial test 2	0.6986	0.5465	0.6423	Passed
Linear-complexity test	0.9946	0.9512	0.9155	Passed

with FONMCO whose entropy source is a chaotic system. The chaotic system used in the paper is fractional order and to the best knowledge of authors there is no this type of study in the literature. The fractional-order chaotic system used in random number generation is as follows.

$$\begin{aligned} \frac{d^{q_x} x}{dt^{q_x}} &= a_1 x + a_2 x^2 + a_3 y \\ \frac{d^{q_y} y}{dt^{q_y}} &= a_4 x + a_5 x^2 - y + z \\ \frac{d^{q_z} z}{dt^{q_z}} &= a_{6y} \end{aligned} \tag{31}$$

q_x, q_y and q_z values are fractional order of the system and all of these values are taken as 0.992. The phase portraits of the system are shown in Fig. 10. The both parameter values and initial conditions of the system are as same as in the non-fractional-order memcapacitor system.

Random number generator design steps with fractional-order chaotic system are as given in Algorithm 1. As it is given in the algorithm, for random number generation, order of the chaotic system and its parameter and initial values are needed. Any change in these parameters will result in generation of different random numbers. The addition of fractional order to the random number generation is an important factor for security. If the generated random numbers are used in encryption, the fractional order of the chaotic system has to be known exactly to regenerate the same random numbers. As a next step, after entering initial and parameter values, time step is determined in order to discretize time series of the fractional-order chaotic system and then discretized with RK4 which is differential equation solving method.

After the discretization process, the obtained floating-based x, y and z outputs is converted into 32-bit binary number; hence, random number generation process is realized. For the random number generation, the last 16 bits of output x, the last 12 bits of output y and the last 16 bits of output z are taken.

To evaluate the performance of the generated number series, NIST-800-22 tests [96] are employed. The NIST test is the most widely used test to evaluate randomness of the number series. In order to be considered successful in passing the NIST-800-22 tests, the P value must be greater than 0.001 for the all tests. The NIST-800-22 tests results of generated numbers from x, y and z outputs are given in Table 2.

Algorithm 1 Random Number Generation Algorithm Pseudo Code

```
1:  Start
2:  Entering system parameters and initial condition of chaotic systems
3:  Entering system fractional orders for x, y and z
4:  Sampling with determination Δh value
5:  while (least 1MBit data) do
6:      Solving the chaotic system using RK4 algorithm
7:      Obtaining time series as float numbers (x, y and z)
8:      Convert float to 32 bit binary numbers
9:   Select LSB-16 bit least binary numbers from RNG from x phase
10:  Select LSB-12 bit least binary numbers from RNG from y phase
11:  Select LSB-16 bit least binary numbers from RNG from z phase
12: end while
13: The implementation of NIST Tests for each 1MBit data
14: if (test results == passed) then
15:     Successful results
16: else {test results == false}
17:     Go to step 9.
18: end if
19: Ready tested random numbers for different RNG applications
20: End
```

9 Conclusions

A memcapacitor chaotic oscillator with two unstable equilibrium points is proposed and investigated. Dynamic properties of the proposed system are investigated. The fractional-order model of the proposed chaotic oscillator is derived and analyzed. The largest Lyapunov exponent of the system is found to exist in the fractional order. Adomian decomposition method is used to discretize the fractional-order system for implementing in FPGA. The fractional-order FPGA-implemented chaotic oscillator is investigated, and the power consumption analysis confirms the existence of the systems' largest Lyapunov exponent in its fractional order.

Acknowledgements This work was partially supported by Sakarya University Scientific Research Projects Unit under Grants 2016-09-00-008, 2016-50-01-026. It was also partially supported by Iran National Science Foundation (No. 96000815). The authors thank Mr. Soroush Dehghan and Mr. Navid Hasanzadeh for help and comments which enhanced the quality of this paper.

References

1. Jafari, S., Sprott, J.C., Golpayegani, S.M.R.H.: Elementary quadratic chaotic flows with no equilibria. Phys. Lett. A **377**(9), 699–702 (2013)
2. Wei, Z.: Dynamical behaviors of a chaotic system with no equilibria. Phys. Lett. A **376**(2), 102–108 (2011)
3. Molaie, M., Jafari, S., Sprott, J.C., Golpayegani, S.M.R.H.: Simple chaotic flows with one stable equilibrium. Int. J. Bifurc. Chaos **23**(11), 1350188 (2013)
4. Wang, X., Chen, G.: A chaotic system with only one stable equilibrium. Commun. Nonlinear Sci. Numer. Simul. **17**(3), 1264–1272 (2012)
5. Barati, K., Jafari, S., Sprott, J.C., Pham, V.-T.: Simple chaotic flows with a curve of equilibria. Int. J. Bifurc. Chaos **26**(12), 1630034 (2016)
6. Jafari, S., Sprott, J.C., Molaie, M.: A simple chaotic flow with a plane of equilibria. Int. J. Bifurc. Chaos **26**(06), 1650098 (2016)
7. Jafari, S., Sprott, J.C., Pham, V.-T., Volos, C., Li, C.: Simple chaotic 3D flows with surfaces of equilibria. Nonlinear Dyn **86**(2), 1349–1358 (2016)
8. Wei, Z., Sprott, J.C., Chen, H.: Elementary quadratic chaotic flows with a single non-hyperbolic equilibrium. Phys. Lett. A **379**(37), 2184–2187 (2015)
9. Wei, Z., Zhang, W., Yao, M.: On the periodic orbit bifurcating from one single non-hyperbolic equilibrium in a chaotic jerk system. Nonlinear Dyn **82**(3), 1251–1258 (2015)

10. Wang, L.: 3-scroll and 4-scroll chaotic attractors generated from a new 3-d quadratic autonomous system. Nonlinear Dyn **56**(4), 453–462 (2009)
11. Munoz-Pacheco, J.M., Tlelo-Cuautle, E., Toxqui-Toxqui, I., Sanchez-Lopez, C., TrejoGuerra, R.: Frequency limitations in generating multi-scroll chaotic attractors using cfoas. Int. J. Electron. **101**(11), 1559–1569 (2014)
12. Tlelo-Cuautle, E., Rangel-Magdaleno, J.J., Pano-Azucena, A.D., Obeso-Rodelo, P.J., Nunez-Perez, J.C.: FPGA realization of multi-scroll chaotic oscillators. Commun. Nonlinear Sci. Numer. Simul **27**(1), 66–80 (2015)
13. Lai, Q., Chen, S.: Generating multiple chaotic attractors from sprott b system. Int. J. Bifurc. Chaos **26**(11), 1650177 (2016)
14. Kengne, J., Negou, A.N., Tchiotsop, D.: Antimonotonicity, chaos and multiple attractors in a novel autonomous memristor-based jerk circuit. Nonlinear Dyn **88**(4), 2589–2608 (2017)
15. Sharma, P.R., Shrimali, M.D., Prasad, A., Kuznetsov, N.V., Leonov, G.A.: Control of multistability in hidden attractors. Eur. Phys. J. Spec. Top. **224**(8), 1485–1491 (2015)
16. Li, C., Hu, W., Sprott, J.C., Wang, X.: Multistability in symmetric chaotic systems. Eur. Phys. J. Spec. Top. **224**(8), 1493–1506 (2015)
17. Sprott, J.C.: Symmetric time-reversible flows with a strange attractor. Int. J. Bifurc. Chaos **25**(05), 1550078 (2015)
18. Sprott, J.C.: Simplest chaotic flows with involutional symmetries. Int. J. Bifurc. Chaos **24**(01), 1450009 (2014)
19. Brummitt, C.D., Sprott, J.C.: A search for the simplest chaotic partial differential equation. Phys. Lett. A **373**(31), 2717–2721 (2009)
20. Gottlieb, H.P.W., Sprott, J.C.: Simplest driven conservative chaotic oscillator. Phys. Lett. A **291**(6), 385–388 (2001)
21. Sprott, J.C.: Simple chaotic systems and circuits. Am. J. Phys. **68**(8), 758–763 (2000)
22. Sprott, J.C.: Some simple chaotic flows. Phys. Rev. E **50**(2), R647 (1994)
23. Chua, L.: Memristor-the missing circuit element. IEEE Trans. Circuit Theory **18**(5), 507–519 (1971)
24. Buscarino, A., Fortuna, L., Frasca, M., Gambuzza, L.V.: A gallery of chaotic oscillators based on HP memristor. Int. J. Bifurc. Chaos **23**(05), 1330015 (2013)
25. Barboza, R., Chua, L.O.: The four-element chua's circuit. Int. J. Bifurc. Chaos **18**(04), 943–955 (2008)
26. Bao, B.-C., Liu, Z., Xu, J.-P.: Dynamical analysis of memristor chaotic oscillator (2010). http://wulixb.iphy.ac.cn/EN/abstract/abstract17028.shtml
27. Chua, L.O., Kang, S.M.: Memristive devices and systems. Proc IEEE **64**(2), 209–223 (1976)
28. Buscarino, A., Fortuna, L., Frasca, M., Gambuzza, L.V.: A chaotic circuit based on hewlett-packard memristor. Chaos Interdiscip. J. Nonlinear Sci. **22**(2), 023136 (2012)
29. Hong, Q.-H., Li, Z.-J., Zeng, J.-F., Zeng Y.-C.: Design and simulation of a memristor chaotic circuit based on current feedback op amp (2014)
30. Muthuswamy, B.: Implementing memristor based chaotic circuits. Int. J. Bifurc. Chaos **20**(05), 1335–1350 (2010)
31. Corinto, F., Krulikovskyi, V., Haliuk, S.D.: Memristor-based chaotic circuit for pseudo-random sequence generators. In: Electrotechnical Conference (MELECON), 2016 18th Mediterranean, pp. 1–3. IEEE (2016)
32. Baleanu, D., Diethelm, K., Scalas, E., Trujillo, J.J.: Fractional Calculus: Models and Numerical Methods, vol. 5. World Scientific, Singapore (2016)
33. Zhou, Y., Wang, J.R., Zhang, L.: Basic Theory of Fractional Differential Equations. World Scientific, Singapore (2016)
34. Diethelm, Kai: The Analysis of Fractional Differential Equations: An Application-Oriented Exposition Using Differential Operators of Caputo Type. Springer, Berlin (2010)
35. Aghababa, M.P.: Robust finite-time stabilization of fractional-order chaotic systems based on fractional lyapunov stability theory. J. Comput. Nonlinear Dyn. **7**(2), 021010 (2012)
36. Boroujeni, E.A., Momeni, H.R.: Non-fragile nonlinear fractional order observer design for a class of nonlinear fractional order systems. Signal Process. **92**(10), 2365–2370 (2012)
37. Zhang R., Gong J. (2014) Synchronization of the fractional-order chaotic system via adaptive observer. Syst. Sci. Control Eng. Open Access J. 2(1):751–754
38. Rajagopal, K., Guessas, L., Karthikeyan, A., Srinivasan, A., Adam, G.: Fractional order memristor no equilibrium chaotic system with its adaptive sliding mode synchronization and genetically optimized fractional order pid synchronization. Complexity **2017**, (2017)
39. Rajagopal, K., Karthikeyan, A., Srinivasan, A.K.: FPGA implementation of novel fractional-order chaotic systems with two equilibriums and no equilibrium and its adaptive sliding mode synchronization. Nonlinear Dyn. **87**(4), 2281–2304 (2017)
40. Rajagopal, K., Guessas, L., Vaidyanathan, S., Karthikeyan, A., Srinivasan, A.: Dynamical analysis and FIGA implementation of a novel hyperchaotic system and its synchronization using adaptive sliding mode control and genetically optimized PID control. Math. Probl. Eng. **2017**, 7307452 (2017) . https://doi.org/10.1155/2017/7307452
41. Rajagopal, K., Karthikeyan, A., Duraisamy, P.: Hyperchaotic chameleon: fractional order FPGA implementation. Complexity (in press) https://www.hindawi.com/journals/complexity/aip/8979408
42. Tlelo-Cuautle, E., Pano-Azucena, A.D., Rangel-Magdaleno, J.J., Carbajal-Gomez, V.H., Rodriguez-Gomez, G.: Generating a 50-scroll chaotic attractor at 66 mhz by using fpgas. Nonlinear Dyn. **85**(4), 2143–2157 (2016)
43. Wang, Q., Yu, S., Li, C., Lü, J., Fang, X., Guyeux, C., Bahi, J. M.: (2016) Theoretical design and FPGA-based implementation of higher-dimensional digital chaotic systems. IEEE Trans. Circuits Syst. I Regul. Pap. **63**(3):401–412
44. Dong, E., Liang, Z., Du, S., Chen, Z.: Topological horseshoe analysis on a four-wing chaotic attractor and its fpga implement. Nonlinear Dyn. **83**(1–2), 623–630 (2016)
45. Tlelo-Cuautle, E., Carbajal-Gomez, V.H., Obeso-Rodelo, P.J., Rangel-Magdaleno, J.J., Nunez-Perez, J.C.: FPGA realization of a chaotic communication system applied to image processing. Nonlinear Dyn. **82**(4), 1879–1892 (2015)
46. Rashtchi, V., Nourazar, M.: FPGA implementation of a real-time weak signal detector using a duffing oscillator. Circuits Syst. Signal Process. **34**(10), 3101–3119 (2015)
47. Wang, G.-Y., Jin, P.-P., Wang, X.-W., Shen, Y.-R., Yuan, F., Wang, X.-Y.: A flux-controlled model of meminductor and its application in chaotic oscillator. Chin. Phys. B **25**(9), 090502 (2016)

48. Pershin, Y.V., Di Ventra, M.: Emulation of floating memcapacitors and meminductors using current conveyors. Electron. Lett. **47**(4), 243–244 (2011)
49. Yu, D.S., Liang, Y., Chen, H., Iu, H.H.C.: Design of a practical memcapacitor emulator without grounded restriction. IEEE Trans. Circuits Syst. II Exp. Briefs **60**(4), 207–211 (2013)
50. Fitch, A.L., Iu, H.H.C., Yu, D.S.: Chaos in a memcapacitor based circuit. In: Circuits and Systems (ISCAS), 2014 IEEE International Symposium on, pp. 482–485. IEEE (2014)
51. Rajagopal, K., Akgul, A., Jafari, S., Karthikeyan, A., Koyuncu, I.: Chaotic chameleon: Dynamic analyses, circuit implementation, fpga design and fractionalorder form with basic analyses. Chaos Solitons Fractals **103**, 476–487 (2017)
52. Pham, V.-T., Volos, C., Jafari, S., Wang, X., Vaidyanathan, S.: Hidden hyperchaotic attractor in a novel simple memristive neural network. Optoelectron. Adv. Mater. Rapid. Commun. **8**(11–12), 1157–1163 (2014)
53. Pham, V.T., Jafari, S., Vaidyanathan, S., Volos, C., Wang, X.: A novel memristive neural network with hidden attractors and its circuitry implementation. Sci. China Technol. Sci. **59**(3), 358–363 (2016)
54. Pham, V.-T., Vaidyanathan, S., Volos, C.K., Jafari, S., Kuznetsov, N.V., Hoang, T.M.: A novel memristive time-delay chaotic system without equilibrium points. Eur. Phys. J. Spec. Top. **225**(1), 127–136 (2016)
55. Wei, Z., Pehlivan, I.: Chaos, coexisting attractors, and circuit design of the generalized sprott c system with only two stable equilibria. Optoelectron. Adv. Mater. Rapid Commun. **6**(7–8), 742–745 (2012)
56. Shahzad, M., Pham, V.-T., Ahmad, M.A., Jafari, S., Hadaeghi, F.: Synchronization and circuit design of a chaotic system with coexisting hidden attractors. Eur. Phys. J. Spec. Top. **224**(8), 1637–1652 (2015)
57. Kengne, J., Njitacke, Z.T., Negou, A.N., Tsostop, M.F., Fotsin, H.B.F.: Coexistence of multiple attractors and crisis route to chaos in a novel chaotic jerk circuit. Int. J. Bifurc. Chaos **26**(05), 1650081 (2016)
58. Bao, B., Jiang, T., Xu, Q., Chen, M., Wu, H., Hu, Y.: Coexisting infinitely many attractors in active band-pass filter-based memristive circuit. Nonlinear Dyn. **86**(3), 1711–1723 (2016)
59. Bao, B.-C., Xu, Q., Bao, H., Chen, M.: Extreme multistability in a memristive circuit. Electron. Lett. **52**(12), 1008–1010 (2016)
60. Bao, B.C., Bao, H., Wang, N., Chen, M., Xu, Q.: Hidden extreme multistability in memristive hyperchaotic system. Chaos Solitons Fractals **94**, 102–111 (2017)
61. Bao, B., Jiang, T., Wang, G., Jin, P., Bao, H., Chen, M.: Two-memristorbased chuas hyperchaotic circuit with plane equilibrium and its extreme multistability. Nonlinear Dyn. **89**, 1157 (2017). https://doi.org/10.1007/s11071-017-3507-0
62. Wang G, Shi C, Wang X, Yuan F.: Coexisting oscillation and extreme multistability for a memcapacitor-based circuit. Math. Probl. Eng. **2017**, 6504969 (2017). https://doi.org/10.1155/2017/6504969
63. Wang, G., Jiang, S., Wang, X., Shen, Y., Yuan, F.: A novel memcapacitor model and its application for generating chaos. Math. Probl. Eng. **2016**, (2016)
64. Leenaerts, D.M.W.: Higher-order spectral analysis to detect power-frequency mechanisms in a driven chua's circuit. Int. J. Bifurc. Chaos **7**(06), 1431–1440 (1997)
65. Pradhan, C., Jena, S.K., Nadar, S.R., Pradhan, N.: Higher-order spectrum in understanding nonlinearity in EEG rhythms. Comput. Math. Methods Med. **2012**, 206857 (2012). https://doi.org/10.1155/2012/206857
66. Pezeshki, C., Elgar, S., Krishna, R.C.: Bispectral analysis of possessing chaotic motion. J. Sound Vib. **137**(3), 357–368 (1990)
67. Li, C., Pehlivan, I., Sprott, J.C., Akgul, A.: A novel four-wing strange attractor born in bistability. IEICE Electron. Exp. **12**(4), 1–12 (2015)
68. Akgul, A., Calgan, H., Koyuncu, I., Pehlivan, I., Istanbullu, A.: Chaosbased engineering applications with a 3d chaotic system without equilibrium points. Nonlinear Dyn. **84**(2), 481–495 (2016)
69. Akgul, A., Pehlivan, I.: A new three-dimensional chaotic system without equilibrium points, its dynamical analyses and electronic circuit application. Tech. Gazette **23**(1), 209–214 (2016)
70. Akgul, A., Moroz, I., Pehlivan, I., Vaidyanathan, S.: A new fourscroll chaotic attractor and its engineering applications. Optik Int. J. Light Electron Opt. **127**(13), 5491–5499 (2016)
71. Akgul, A., Hussain, S., Pehlivan, I.: A new three-dimensional chaotic system, its dynamical analysis and electronic circuit applications. Optik Int. J. Light Electron Opt. **127**(18), 7062–7071 (2016)
72. Jafari, M.A., Mliki, E., Akgul, A., Pham, V.-T., Kingni, S.T., Wang, X., Jafari, S.: Chameleon: the most hidden chaotic flow. Nonlinear Dyn. **88**, 2303 (2017). https://doi.org/10.1007/s11071-017-3378-4
73. Hu, W., Akgul, A., Li, C., Zheng, T., Li, P.: A switchable chaotic oscillator with two amplitude-frequency controllers. J. Circuits Syst. Comput. **26**(10), 1750158 (2017)
74. Wei, Z., Moroz, I., Sprott, J.C., Akgul, A., Zhang, W.: Hidden hyperchaos and electronic circuit application in a 5d self-exciting homopolar disc dynamo. Chaos Interdiscip. J. Nonlinear Sci. **27**(3), 033101 (2017)
75. Kai, G., Zhang, W., Wei, Z.C., Wang, J.F., Akgul, A.: Hopf bifurcation, positively invariant set, and physical realization of a new four-dimensional hyperchaotic financial system. Math. Probl. Eng. **2017**, (2017)
76. Volos, C., Akgul, A., Pham, V.-T., Stouboulos, I., Kyprianidis, I.: A simple chaotic circuit with a hyperbolic sine function and its use in a sound encryption scheme. Nonlinear Dyn. **89**, 1047 (2017). https://doi.org/10.1007/s11071-017-3499-9
77. Akgul, A., Li, C., Pehlivan, I.: Amplitude control analysis of a four-wing chaotic attractor, its electronic circuit designs and microcontroller-based random number generator. J. Circuits Syst. Comput. **26**, 1750190 (2017). https://doi.org/10.1142/S0218126617501900
78. Charef, A., Sun, H.H., Tsao, Y.Y., Onaral, B.: Fractal system as represented by singularity function. IEEE Trans. Autom. Control **37**(9), 1465–1470 (1992)
79. Adomian, G.: A review of the decomposition method and some recent results for nonlinear equations. Math. Comput. Model. **13**(7), 17–43 (1990)

80. Sun, H.H., Abdelwahab, A., Onaral, B.: Linear approximation of transfer function with a pole of fractional power. IEEE Trans. Autom. Control **29**(5), 441–444 (1984)
81. Tavazoei, M.S., Haeri, M.: Unreliability of frequency-domain approximation in recognising chaos in fractional-order systems. IET Signal Process. **1**(4), 171–181 (2007)
82. Shao-Bo He, Ke-Hui Sun, and Hui-Hai Wang. Solution of the fractional-order chaotic system based on adomian decomposition algorithm and its complexity analysis (2014). http://wulixb.iphy.ac.cn/EN/abstract/abstract57588.shtml
83. Caponetto, R., Fazzino, S.: An application of adomian decomposition for analysis of fractional-order chaotic systems. Int. J. Bifurc. Chaos **23**(03), 1350050 (2013)
84. He, S., Sun, K., Wang, H.: Complexity analysis and dsp implementation of the fractional-order lorenz hyperchaotic system. Entropy **17**(12), 8299–8311 (2015)
85. Bratley, P., Fox, B.L., Schrage, L.E.: A Guide to Simulation. Springer, Berlin (2011)
86. Jacoboni, C., Lugli, P.: The Monte Carlo Method for Semiconductor Device Simulation. Springer, Berlin (2012)
87. Akgul, A., Kacar, S., Aricioglu, B., Pehlivan, I.: Text encryption by using one-dimensional chaos generators and nonlinear equations. In: Electrical and Electronics Engineering (ELECO), 2013 8th International Conference on, pp. 320–323. IEEE (2013)
88. Tuncer, T., Avaroglu, E., Turk, M., Ozer, A.B.: Implementation of nonperiodic sampling true random number generator on FPGA. J. Microelectron. Electron. Compon. Mater. **44**(4), 296–302 (2014)
89. Vasyltsov, I., Hambardzumyan, E., Kim, Y.-S., Karpinskyy, B.: Fast digital trng based on metastable ring oscillator. In: International Workshop on Cryptographic Hardware and Embedded Systems, pp. 164–180. Springer (2008)
90. Ergun, S., Ozoguz, S: A chaos-modulated dual oscillator-based truly random number generator. In: Circuits and Systems, 2007. ISCAS 2007. IEEE International Symposium on, pp. 2482–2485. IEEE (2007)
91. Yalcin ME, Suykens JAK, Vandewalle J (2004) True random bit generation from a double-scroll attractor. IEEE Trans. Circuits Syst. I Regul. Pap. 51(7):1395–1404
92. Stojanovski T, Kocarev L (2001) Chaos-based random number generators-part i: analysis [cryptography]. IEEE Trans. Circuits Syst. I Fundam. Theory Appl. 48(3):281–288
93. Stojanovski T., Pihl J., Kocarev L. (2001) Chaos-based random number generators-Part ii: practical realization. IEEE Trans. Circuits Syst. I Fundam. Theory Appl. 48(3):382–385
94. Callegari, S., Rovatti, R., Setti, G.: Embeddable adc-based true random number generator for cryptographic applications exploiting nonlinear signal processing and chaos. IEEE Trans. Signal Process. **53**(2), 793–805 (2005)
95. Çavuşoğlu, Ü., AkgÜl, A., Kaçar, S., Pehlivan, I., Zengin, A.: A novel chaos-based encryption algorithm over TCP data packet for secure communication. Secur. Commun. Netw **9**(11), 1285–1296 (2016)
96. Rukhin, A., Soto, J., Nechvatal, J., Barker, E., Leigh, S., Levenson, M., Banks, D., Heckert, A., Dray, J., Vo, S. et al.: Statistical test suite for random and pseudorandom number generators for cryptographic applications, NIST special publication. (2010)